Journal of Medical Systems (2019) 43: 299
https://doi.org/10.1007/s10916-019-1427-x

IMAGE & SIGNAL PROCESSING

A Two Layer Sparse Autoencoder for Glaucoma Identification with Fundus Images

U. Raghavendra[1] · Anjan Gudigar[1] · Sulatha V. Bhandary[2] · Tejaswi N. Rao[1] · Edward J. Ciaccio[3] · U. Rajendra Acharya[4,5,6]

Received: 20 December 2018 / Accepted: 21 July 2019 / Published online: 30 July 2019

Abstract
Glaucoma is a type of eye condition which may result in partial or consummate vision loss. Higher intraocular pressure is the leading cause for this condition. Screening for glaucoma and early detection can avert vision loss. Computer aided diagnosis (CAD) is an automated process with the potential to identify glaucoma early through quantitative analysis of digital fundus images. Preparing an effective model for CAD requires a large database. This study presents a CAD tool for the precise detection of glaucoma using a machine learning approach. An autoencoder is trained to determine effective and important features from fundus images. These features are used to develop classes of glaucoma for testing. The method achieved an $F-measure$ value of 0.95 utilizing 1426 digital fundus images (589 control and 837 glaucoma). The efficacy of the system is evident, and is suggestive of its possible utility as an additional tool for verification of clinical decisions.

Keywords CAD · Cascade · Glaucoma · Sparse autoencoder

Introduction

Glaucoma is an ocular condition which mainly affects the optical nerves, and when left untreated, eventually causes blindness. According to the Glaucoma Research Foundation, glaucoma is the leading cause of blindness (https://www.glaucoma.org/glaucoma/glaucoma-facts-and-stats.php). The optic nerve has approximately 1 million individual nerve fibers which are responsible for transmission of visual signals between eye and brain. Primary open-angle glaucoma is the most common form wherein one can observe very high fluid pressure. This increase in pressure may cause progressive damage to the optic nerve and a loss of nerve fibres. The fluid pressure inside the eye is the intraocular pressure (IOP) [1–3]. The optic nerve captures images and sends them to the brain. Raised IOP causes optic nerve damage leading to visual field defects and eventual blindness. Heredity plays a role in the occurrence of glaucoma. Glaucoma often manifests in the later stages of life due to heredity. Hence it is recommended to have one's eyes checked each year, for those individuals above the age of 40. However, glaucoma can even occur in teenagers, children, and infants (https://www.webmd.com/eye-health/medical-reference). The probability of glaucoma in a diabetic patient is increased; hence all such patients are advised to have their eyes checked regularly. The block in fluid (aqueous humour) within the eye leads to an increase in IOP, which causes optic nerve damage [4, 5]. Neuroretinal rim defects are evident as the initial features of optic nerve damage. This layer will be thickest near the optic disc, and it diminishes toward the ora serrata, as per ISNT rule [6]. Defects in the neuroretinal rim become readily apparent by

This article is part of the Topical Collection on *Image & Signal Processing*

✉ Anjan Gudigar
anjan.gudigar@manipal.edu

[1] Department of Instrumentation and Control Engineering, Manipal Institute of Technology, Manipal Academy of Higher Education, Manipal 576104, India

[2] Department of Ophthalmology, Kasturba Medical College, Manipal Academy of Higher Education, Manipal 576104, India

[3] Department of Medicine, Columbia University, New York, NY, USA

[4] Department of Electronics and Computer Engineering, Ngee Ann Polytechnic, Clementi 599489, Singapore

[5] Department of Biomedical Engineering, School of Science and Technology, SUSS University, Clementi 599491, Singapore

[6] School of Medicine, Faculty of Health and Medical Sciences, Taylor's University, Subang Jaya, Malaysia

measuring the cup-to-disc ratio (CDR) [7]. The ideal CDR value for the human eye is 0.3 [2, 8]. It is currently difficult to identify this illness in its initial stages as it is asymptomatic. Thus, the development of computer aided diagnosis (CAD) tools have become a major research focus to obtain an early and automated glaucoma detection system.

In recent years, many methods were proposed for glaucoma classification. Most of the algorithms incorporate feature extraction and classification technology. Feature extraction has been implemented in previous related work using the wavelet transform [9–13], the Gabor transform [14], and higher order spectral analysis (HOS) [15–17]. Many machine learning and neural network schemes such as the artificial neural network (ANN) [18–20], support vector machine (SVM) [9, 10, 14], and *k*-nearest neighbor (*k*-NN) [21–23] have been employed for classification of glaucoma. Recently there were several techniques proposed which utilize big data. Chen et al. made use of 1676 images and achieved an area under curve (AUC) of 0.887 for glaucoma detection using a convolutional neural network (CNN) and ROI (i.e., region of interest) [24]. In [25] an expert system was developed using GIST and SVM which achieved a 97% accuracy level from a pool of 1000 fundus images. The same research group has recently proposed a powerful model for glaucoma detection, which can even classify during the initial stages, using a CNN with 18 layers, and making use of 1426 digital fundus images. This technique achieved a maximum accuracy of 98.13% [26]. The most recent studies and methodologies are summarized in Table 1.

From the literature, it is observed that CAD tools for glaucoma detection are developed by researchers using both handcrafted features and CNN modules. However, design of feature learning algorithms is tedious, and the designer must have appropriate knowledge of handcrafted features. The CNNs have shown remarkable performance on big datasets when used with various tuning parameters. Yet some of these algorithms are not particularly feasible for use with the larger datasets because of feature impartiality. To overcome this impediment and enhance classification, a more powerful algorithm would be needed. Such a system is described herein, with the following two key factors:

- Effective utilization of an autoencoder, for the successful identification of glaucoma, while avoiding manual feature extraction methods.
- Use of a large dataset with multiple cases of control versus the glaucoma condition.

The remainder of this paper is arranged as follows. Section 2 provides background theory for sparse autoencoders, and proposed methodology with the utilized materials. The experimental results are presented in Section 3. Discussion of the results and concluding remarks are given in Sections 4 and 5, respectively.

Approach using a sparse autoencoder

Dataset

The created dataset consists of 1426 retinal fundus images, of which 589 are control and 837 are glaucoma images. It includes 294 normal and 418 glaucoma subjects; however one subject had unilateral glaucoma. Hence the respective images are included in both glaucoma and normal subjects. All images were collected from Kasturba Medical College, Manipal, India. Institutional ethical approval was obtained for capture of all fundus images analysed for the study. Normal fundus images were acquired from patients visiting for a routine health check-up. Images were collected from glaucoma patients having vision problems, and these were categorized as mild, moderate and severe, after a detailed clinical examination by experts. The images were acquired from the age group of 20–70 years, during the last five years. The fundus camera Zeiss FF 450 was used for image capture, and images were then converted to the jpeg format for processing, which has a negligible effect on the model performance. The database, which is used in this study, is comparatively large and diverse as compared to public databases. Sample images are shown in Fig. 1.

Methodology

The ultimate aim of this work was to categorize normal versus affected eye. We propose the following structure, containing cascading autoencoders, as depicted in Fig. 2. Here, two autoencoders are cascaded, and then combined using a Softmax layer. Three components were trained separately; unlike autoencoders, Softmax is trained in a supervised way using training labels. Regularizers such as L2Weight (L2W) regularization, sparsity regularization, and sparsity proportion are used by the autoencoder, depending on the nature of the application.

Sparse autoencoder

Autoencoders are useful for unsupervised learning. They are designed to learn a low-dimensional representation from a higher-dimensional dataset [34–36]. With the limited capacity, the model is forced to form a very efficient encoding of the data that is essentially the low-dimensional code (please refer to Fig. 3).

The encoder and decoder may have multiple layers; however for each instance a single layer is considered. The input vector x can be mapped to another vector z by the encoder as

Table 1 Comparison of the proposed methodology with existing works

Paper	Description	#images	Performance (%)
[18]	CDR and ANN classifier is used.	61	GSn: 100 GSp: 80
[27]	Histogram based features are used.	–	CDR Error: 0.091
[20]	Self-organizing maps are used.	127	CR: 87.50
[22]	Independent component analysis and *k*-NN classifier is used.	120	GA: 91
[10]	Empirical wavelet transform, correntropy and LS-SVM classifier.	555	GA(Three fold): 98.33
[13]	Wavelet energy features are used with probabilistic neural network classifier.	–	95%
[28]	Wavelet based energy features and sequential minimal optimization are used.	60	GA: 93
[11]	Wavelet energy features and classifier ANN is used.	–	GA: 97.6
[12]	Wavelet and geometric moment features and classifiers such as SVM, *k*-NN, error back-propagation training algorithm are used.	350	GA: 86.57
[15]	HOS cumulants features and Naïve Bayesian classifier is used.	272	GA: 84.72 (2 class) GA: 92.65 (3 class) GSn: 100
[29]	HOS bispectrum and random forest are used.	60	GA:91
[16]	HOS, trace transform and discrete wavelet transform (DWT) and SVM classifier are used.	60	GA: 91.67 GSn: 90 GSp: 93.33
[9]	HOS and DWT based features, SVM classifier are used.	60	GA: 95.00 GSn: 93.33 GSp: 96.67
[30]	Hough transform, linear discriminant analysis (LDA) and classification trees.	–	GA: 72.3
[31]	Circular Hough transform and unsupervised classification.	325	CDR error: 0.10
[21]	Haralick texture features and classifier *k*-NN is used.	60	GA: 98
[23]	Local configuration pattern and texton along with *k*-NN is used.	702	GA: 95.7 GSn: 96.2 GSp: 93.7
[32]	Variational mode decomposition and entropy with SVM is used.	488	GA: 95.19 GSn: 93.62 GSp: 96.71
[14]	Gabor transform and SVM classifier is used.	510	GA: 93.10 GSn: 89.75 GSp: 96.20
[25]	Radon transform, GIST and locality sensitive discriminant analysis (LSDA) with SVM is used.	1000	GA: 97.00 GSn: 97.80 GSp: 95.80
[33]	Bit-plane slicing and local binary pattern	1426	GA: 99.30 GSn: 98.84 GSp: 99.64
[24]	CNN	1676	AUC:0.887
[26]	CNN (18 layer) and LDA are used.	1426	GA: 98.13 GSn: 98.00 GSp: 98.30
Proposed Method	Sparse autoencoder	1426	GA:95.3% GP:96.76%

*GA-Accuracy, GSn-Sensitivity, GSp-Specificity, Classification rate: CR, GP:Precision

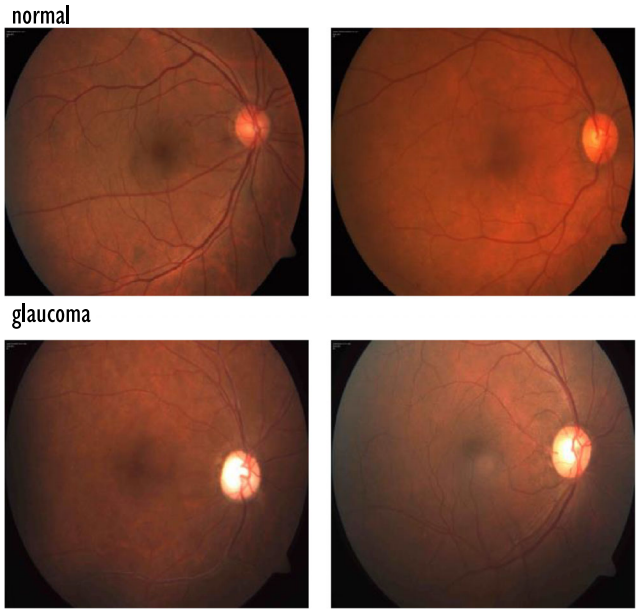

Fig. 1 Sample images used in the current study

$$z = h(Wx + b) \tag{1}$$

where h is the transfer function and it is also a sigmoid function, W is the weight matrix, and b is a bias vector. In the decoding section, the original input vector is estimated as

$$\hat{x} = h'(W'z + b') \tag{2}$$

Further, adding a regularizer to the cost function leads to a possible sparsity of an autoencoder [34]. To limit the average activation value of the hidden-layer neuron, a sparse penalty term is added to the cost function [35]. The cost function is defined as

$$C = (mean\ squared\ error) + \lambda^*(L_2\ \text{regularization}) + \beta^*(sparsity\ regularization)$$

The coefficients λ (i. e., for L2W regularization) and β (*i. e.* for sparsity regularization) are optimally adjusted while training an autoencoder. Training the autoencoder is performed to find the optimal parameters and to reduce the reconstruction error.

Softmax regression

Softmax regression is largely used for supervised learning. This regression is incorporated at a later stage to differentiate the output from the stacked autoencoder into various categorizations.

Herein, (z, l) is a Softmax regression training sample, where z represents the feature vector and $l \in (1, 2)$ represents the class label. The output of the Softmax is defined as

$$g_\theta(z) = \begin{pmatrix} p(l=1) \\ p(l=2) \end{pmatrix} = \frac{1}{\sum_{i=1}^{2} e^{\theta_i^T z}} \begin{pmatrix} e^{\theta_1^T z} \\ e^{\theta_2^T z} \end{pmatrix} \tag{3}$$

where $g_\theta(z)$ is the hypothesis probability vector, θ_1 *and* θ_2 are the model parameters, and

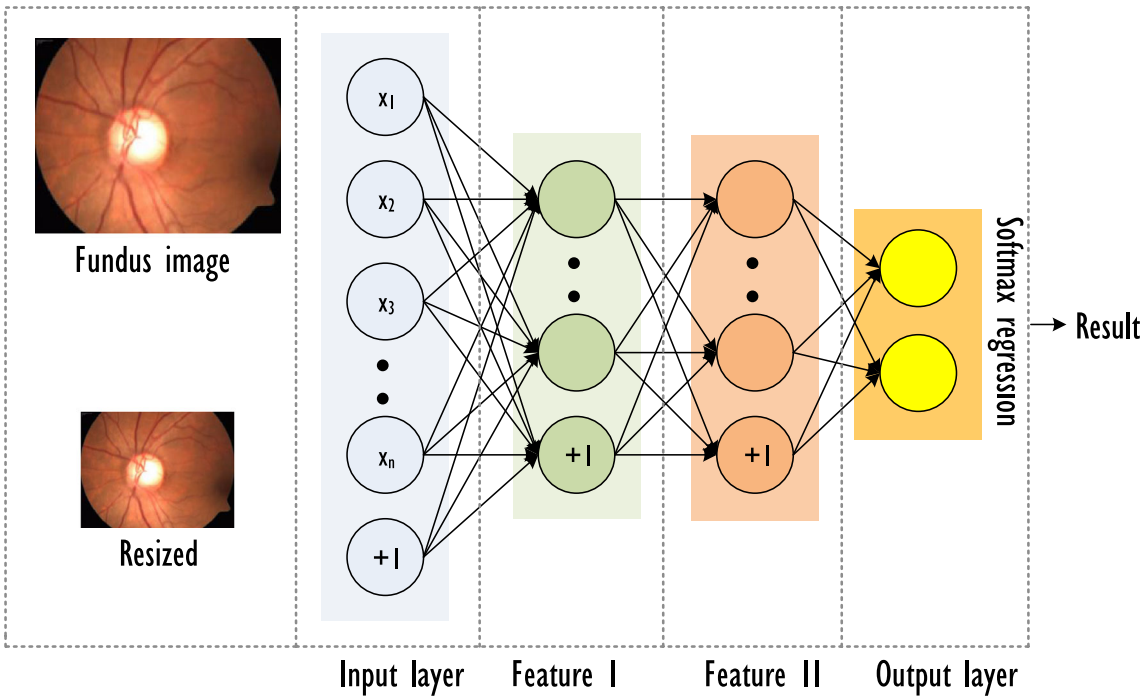

Fig. 2 Graphical illustration of the proposed methodology

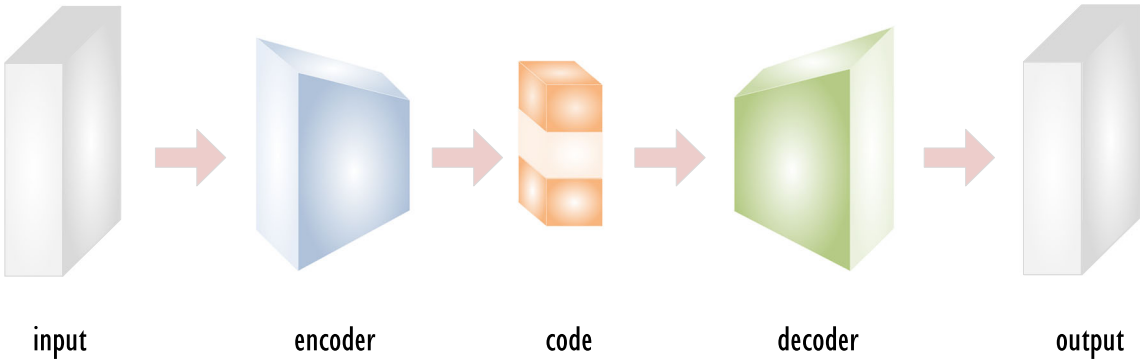

Fig. 3 Architectural view of an autoencoder

$1/\sum_{i=1}^{2} e^{\theta_i^T z}$

normalizes the probability distribution [36, 37].

Working

Instead of adding fundus images directly to the model, which would result in a high computational complexity, the fundus images were rescaled, and then input to a model consisting of a stack of autoencoders. A dataset of 1426 images having a 1024 × 1024 pixel dimension was acquired and then resized to 64×64 pixels. In this study we have included 70% of the images for training and 30% for testing, which translates to 998 training fundus images and 428 test images. Once the images are resized, they are discretely stored in matrix form (training images and testing images are stored in two different matrices). Now labels are stored as per the training and testing images in a matrix. Matrix labelling is done in such a way that in every column the element is set to 1 to denote the class of the corresponding image. Neural network weights, when arbitrarily assigned, can result in differing convergence. In order to eschew this consequence, we initially set the random number generator to default to prevent deviation in the result. The sparse autoencoder utilized for the study incorporates regularizers to learn the sparse representation in the first layer. Next the raw data is input to the 1st sparse autoencoder, thus obtaining primary features. These primary features will then be used as raw input for the 2nd sparse autoencoder to learn secondary features. Hence, each layer's outputs are connected to the successive layer's inputs. After pilot experiments, system parameter values were selected based on highest accuracy achieved; see Section 4. The first hidden layer weighting was thus assigned a value of 20. The first autoencoder was then trained with a weight regularization of 0.04, sparsity regularization of 420, and a sparsity proportion whose value should be between 0 and 1 was assigned to be 0.15 for the glaucoma dataset, with a maximum Epoch of 5. Each image consists of 12288 pixels (data points), and as the images are alimented, the 1st autoencoder assigns features automatically and it reduces the dimensionality of data points from 12288 to 20. The output of the first autoencoder will then be accommodative for input to the second autoencoder (please refer to Fig. 4).

The output from the antecedent autoencoder is then transferred into the second autoencoder, which is designed in a homogeneous fashion similar to the first autoencoder, but the layering has been reduced to 10 so that the second autoencoder learns a more minuscule representation of the image. At this stage, the linear regularization value is 0.02, and the sparsity regularization is 420, with a sparsity proportion of 0.85 and maximum Epoch of 20. A single image in the 1st autoencoder had 12288 input and output nodes (i.e., dimension of 64×64×3 nodes). Secondary features are obtained in this autoencoder, which will serve as raw input for the Softmax layer. The basic structure of the Softmax layer is provided in Fig. 5.

Furthermore, the Softmax layer is then trained for the 10 features of the 2nd autoencoder, with the maximum Epoch being 400. The features are reduced from 12288 to 10, which will increase the Softmax layer efficiency and decrease processing time. The Softmax layer is trained in order to match the secondary features.

Results

The system performance is calculated using accuracy (GA), precision (GP), recall (GR) and *F-measure*. For an instance, we have the number of true positive (TP), number of true negative (TN), number of false positive (FP) and number of false negative (FN); then the preceding can be calculated as:

$$GA = \frac{TP + TN}{TP + FP + TN + FN} \tag{4}$$

$$GP = \frac{TP}{TP + FP} \tag{5}$$

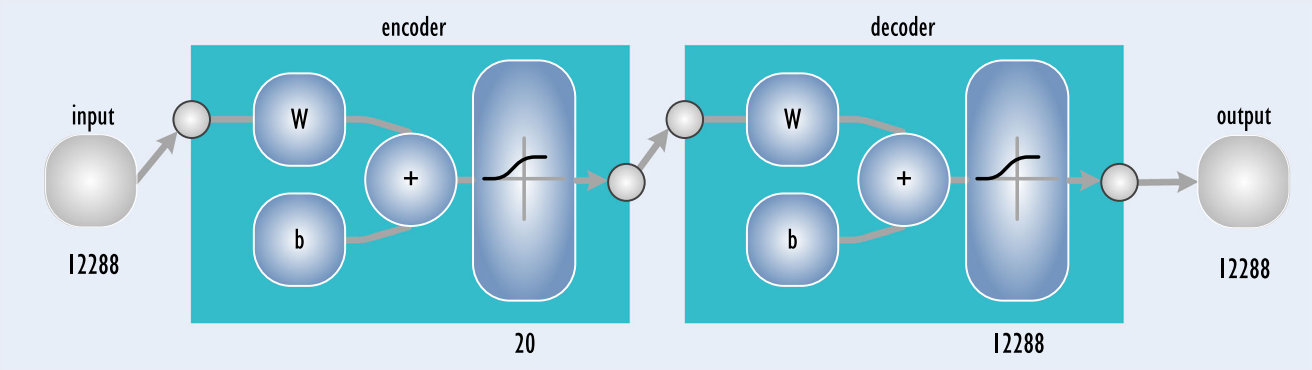

Fig. 4 Architecture of the first autoencoder

$$GR = \frac{TP}{TP + FN} \tag{6}$$

$$F\text{-}measure = 2 \times \frac{GP \times GR}{GP + GR} \tag{7}$$

In order to execute a coherent assessment, all input fundus images were resized to dimension 64 ×64, and were subjected to the autoencoder. The algorithm was run in MATLAB with a configuration: Intel Xeon CPU E3, 16 GB. Variable parameters were empirically fixed based on the repeated experiments.

The characteristics of the two autoencoders require further consideration. Data is stored in matrix form, and is divided into training as well as testing components. The program is run with 1st encoder sparsity proportion, which was set to a value of 0.15, with a varying sparsity proportion for the 2nd autoencoder. Training and testing are performed with initial parameter settings; later the parameters are changed to obtain the highest accuracy. The accuracy and precision were calculated during evolution. A maximum accuracy of 85% was obtained thusly. In the next step, the sparsity proportion that resulted in the maximum value was maintained as constant, and the first autoencoder sparsity proportion was varied. This implementation achieved a 95.3% accuracy and 96.8% precision. The system results in an *F-measure* of 0.95 by obtaining TP = 239, FP = 8, FN = 12 and TN = 169. In total, 499 and 214 subjects were considered during the training and testing process, respectively. The complete training and testing process required 35.68 s to complete. Fig. 6 shows the graph of different sparsity proportions of autoencoders versus model performance (i.e., precision). Table 2 shows the performance of the proposed system in comparison with other classifiers. All of the results shown were evaluated with training and testing partitions of 70 and 30, respectively.

Discussion

In the current study, autoencoders were cascaded for the identification of glaucoma from fundus imagery. It has been observed that stacked autoencoders have outperformed many conventional techniques for CAD [38]. They perform the training operation using neural networks with multiple hidden layers, by training one at a time. We have used two autoencoders to train the hidden layer in an unsupervised way. A further Softmax layer is

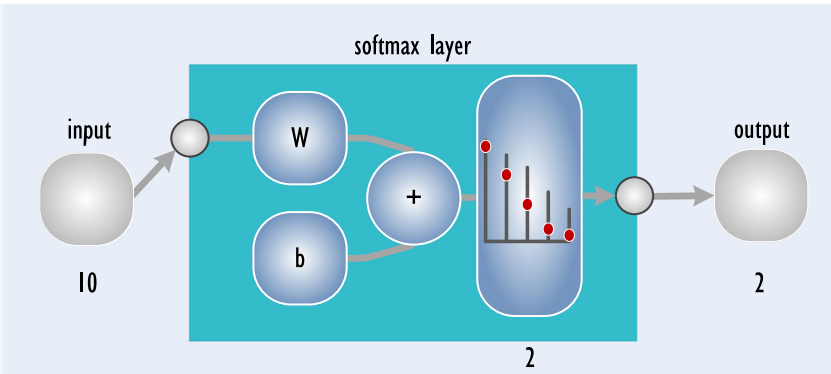

Fig. 5 Architecture of the Softmax layer

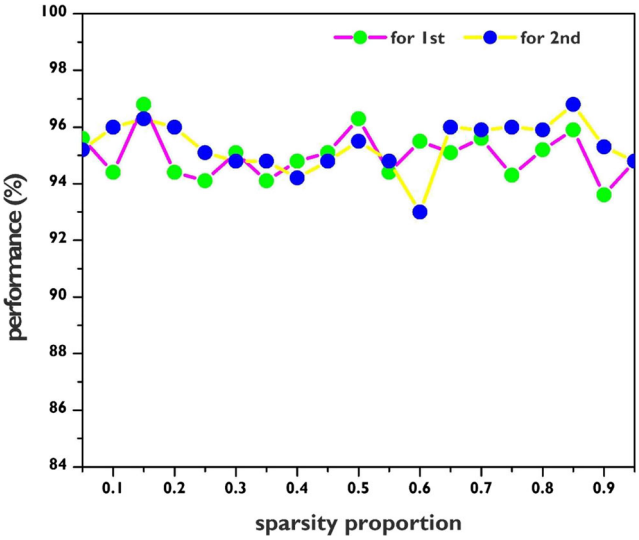

Fig. 6 The plot of sparsity proportion verses performance measure (i.e., precision)

trained and a stacked network is generated by joining the layers. The sparsity is controlled by a sparsity regularizer, and its regulation depends on the nature of the problem. In the current study, a maximum accuracy is achieved using a sparsity proportion equal to 0.15 and 0.85 for the first and second autoencoders, respectively (please refer to Fig. 6). The method achieved a maximum accuracy of 95.3% while misclassifying 20 images from the testing group. The experiment is also conducted for image sizes of 30×30, 40×40, 64×64 and 128×128. It is observed that accuracies of 63.3%, 62.1% and 63.8% were obtained for image sizes of 30×30, 40×40 and 128×128, respectively. The image size of 64×64 achieved the maximum result, and is considered the optimal size for the current study. It is also noted that the number of false negatives and positives produced by the proposed system are comparable. Experiments were conducted to select the best possible L2W and number of epochs to achieve best results. It is noted from Table 3 that L2W:0.04 and epoch: 5 for 1st autoencoder and L2W:0.02 and epoch: 20 for 2nd autoencoder result in maximum accuracy. Hence these parameters are maintained constant for all experiments.

Table 2 Performance comparison of the proposed system with various classifiers

Classifier	GA (%)	GP(%)	GR(%)	*F-measure*
LDA	63.5	73	61	0.66
Linear SVM	70.5	73	80	0.76
Cosine KNN	77.3	81	80	0.80
Autoencoder I	93.9	94.5	95.2	0.94
Autoencoder II	95.3	96.8	95.2	0.95

It is observed that the system misclassifies only 10 subjects from 214, i.e., 4.67%, which indicates the promising performance of the system. Table 2 shows that the proposed system achieved promising results as compared to various classifiers and a single autoencoder. Hence the system achieved comparable results to state-of-the-art techniques. A summary of the obtained performance results for the proposed method, in comparison with existing techniques, is shown in Table 1.

In general, the design of a CAD tool consists of two approaches. The first approach consists of four stages, namely: 1) preprocessing, 2) feature extraction, 3) dimensionality reduction, and 4) classification. Many feature extraction methods are designed by investigators to extract vital information from fundus images [9, 10, 14–16, 21–23, 25]. These features are reduced by various dimensionality reduction techniques, and should have the capability to handle nonlinearities [25]. Further classification algorithms are selected in order to avoid overfitting, and to achieve a maximum classification accuracy. These results are based on the number of images used and the ability of the system to know the underlying structure of the data points. Features such as HOS [9, 15, 16, 29], entropy [10, 32] and LBP [33] are commonly used. It is noted that the combination of GIST and LSDA achieved a better classification accuracy [25]. However, design of feature learning algorithms is tedious, and the designer must have appropriate knowledge of handcrafted features. Yet, some of these algorithms are not particularly feasible for use with the larger datasets because of feature impartiality. The second approach is based on convolutional neural networks (CNNs). The CNNs have shown remarkable performance on big datasets when used with various tuning parameters. They require the proper selection of layers to achieve better results. In [26], 18 layers are used, and further increase of layers may require a large amount of memory. It is also observed that CNNs require a computational platform with high configuration. The major advantage of the CAD method introduced in this study is that it requires minimum tuning parameters as compared to CNNs. It showed equivalent performance as compared to handcrafted methods. It does not require conventional stages such as feature generation, data dimensionality handling, and feature ranking. Another advantage is that preprocessing is not required as an initial stage, thus reducing the time to design an appropriate pipeline structure. It can also readily run on a standalone system with minimum configuration.

This was a first attempt to apply stacked autoencoders to glaucomatous images. In future work, improvement could be done by cascading more networks, with the selection of

Table 3 Selecting L2W and number of epochs for autoencoder I and II based on the accuracy (%)

L2W	**epochs**											
	5		10		15		**20**		25		30	
	I	II	I	II	I	II	I	II	I	II	I	II
0.01	93.7	94.2	94.2	93.5	93.5	94.2	93.0	93.5	93.2	94.9	92.3	93.5
0.02	94.6	94.9	93.0	93.7	93.7	94.4	91.8	**95.3**	93.5	93.9	93.0	93.9
0.03	93.9	94.2	94.9	93.7	92.3	67.5	92.1	95.0	92.3	94.2	92.8	94.2
0.04	**95.3**	95.1	91.8	93.5	93.7	94.9	93.7	93.9	92.5	93.0	91.4	92.8
0.05	94.4	94.4	93.0	93.5	92.5	93.7	92.8	93.7	93.2	94.9	91.6	92.3
0.06	93.7	94.2	93.7	93.9	93.0	93.7	91.8	93.5	93.7	93.0	93.0	94.2
0.07	95.1	94.2	93.2	94.2	93.5	93.2	92.5	94.4	92.5	93.0	91.8	92.8
0.08	94.2	94.6	91.1	93.7	93.0	93.2	91.8	94.6	92.5	91.4	94.2	93.7
0.09	94.4	93.9	93.0	94.4	93.5	94.6	92.1	94.4	92.3	91.6	94.9	93.9
0.10	93.9	94.2	93.2	94.4	93.5	93.7	93.7	91.6	93.9	92.8	93.5	94.2

Bold indicates the highest accuracy

optimal parameters. We would like to combine the segmentation and stacked encoders to enhance classification accuracy as a future goal. We plan to incorporate a convolutional autoencoder by finding clinical features using UNet as a multi centric study. The categorization of different stages of glaucoma is of major concern for future efforts.

Conclusion

Glaucoma is a leading cause of visual impairment. Many people throughout the world become afflicted with this disease. The development of a CAD tool can enable ophthalmologists to detect glaucoma at an earlier, mild stage. In developing countries, the shortage of medical professionals requires that a very reliable CAD system be available to diagnose glaucoma with high accuracy. Since glaucoma is a major cause of visual impairment, its early stage diagnosis is of utmost consequence for the public health. The use of autoencoders is helpful to select features serving as input for succeeding layers, instead of considering the image as a whole. The paradigm introduced in this study avoids image segmentation, and provides required features for classification. Our technique obtained comparable performance measures for a large number of images. The model may be used as an assistive tool for detecting early stage glaucoma, and to help in clinical advising.

Compliance with ethical standards

Conflict of interest None of the authors have any conflict of interest.

Ethical approval This article does not contain any studies with human participants or animals performed by any of the authors.

References

1. Acharya, U. Rajendra., Ng, E. Y. K., and Suri, J. S., *Image Modeling of the Human Eye, Artech House bioinformatics & biomedical imaging series, Artech House*, 2008.
2. Goldmann, H., and Schmidt, T., Applanation tonometry. *Ophthalmologica* 134:221–242, 1957.
3. Hagiwara, Y., Koh, J. E. W., Tan, J. H., Bhandary, S. V., Laude, A., Ciaccio, E. J., Tong, L., and Acharya, U. R., Computer-aided diagnosis of glaucoma using fundus images: A review. *Comput. Methods Prog. Biomed.* 165:1–12, 2018.
4. Sommer, A., Tielsch, J. M., Katz, J., Quigley, H. A., Gottsch, J. D., Javitt, J., and Singh, K., Relationship between intraocular pressure and primary open angle glaucoma among white and black Americans. The Baltimore eye survey. *Arch. Ophthalmol.* 109(8): 1090–1095, 1991.
5. Quigley, H. A., and Broman, A. T., The number of people with glaucoma worldwide in 2010 and 2020. *Br. J. Ophthalmol.* 90(3): 262–267, 2006.
6. Harizman, N., Oliveira, C., Chiang, A., Tello, C., Marmor, M., Ritch, R., and Liebmann, J. M., The ISNT rule and differentiation of normal from glaucomatous eyes. *Arch. Ophthalmol.* 124(11): 1579–1583, 2006.
7. Burgoyne, C. F., *Pearls of glaucoma management*. Berlin, Heidelberg, (Chapter 1. p. 1): *Springer*, 2010.
8. Eye Diseases Prevalence Research Group, Prevalence of open-angle glaucoma among adults in the United States. *Arch. Ophthalmol.* 122:532–538, 2004.
9. Mookiah, M. R. K., Acharya, U. R., Lim, C. M., Petznick, A., and Suri, J. S., Data mining technique for automated diagnosis of glaucoma using higher order spectra and wavelet energy features. *Knowl.-Based Syst.* 33:73–82, 2012.
10. Maheshwari, S., Pachori, R. B., and Acharya, U. R., Automated diagnosis of glaucoma using empirical wavelet transform and correntropy features extracted from fundus images. *IEEE journal of biomedical and health informatics* 21(3):803–813, 2016.
11. Gayathri, R., Rao, P. V., and Aruna, S., Automated glaucoma detection system based on wavelet energy features and ANN. In Advances in Computing, Communications and Informatics (ICACCI, 2014 International Conference on, pp. 2808–2812. IEEE, 2014.

12. Gajbhiye, Gaurav O., and Kamthane, Ashok N., Automatic classification of glaucomatous images using wavelet and moment feature. In India Conference (INDICON), 2015 Annual IEEE, pp. 1–5. IEEE, 2015.
13. Annu, N., and Justin, J., Automated classification of glaucoma images by wavelet energy features. *International Journal of Engineering and Technology* 5(2):1716–1721, 2013.
14. Acharya, U. R., Ng, E. Y. K., Eugene, L. W. J., Noronha, K. P., Min, L. C., Nayak, K. P., and Bhandary, S. V., Decision support system for the glaucoma using Gabor transformation. *Biomedical Signal Processing and Control* 15:18–26, 2015.
15. Noronha, K. P., Acharya, U. R., Prabhakar Nayak, K., Martis, R. J., and Bhandary, S. V., Automated classification of glaucoma stages using higher order cumulant features. *Biomedical Signal Processing and Control* 10:174–183, 2014.
16. Krishnan, M. M. R., and Faust, O., Automated glaucoma detection using hybrid feature extraction in retinal fundus images. *Journal of Mechanics in Medicine and Biology* 13(01):1350011, 2013.
17. Nikias, C. L., and Petropulu, A. P., *Higher-order spectra analysis: A nonlinear signal processing framework*. Englewood Cliffs, NJ: *PTR Prentice Hall*, 1993.
18. Nayak, J., Acharya, R., Subbanna Bhat, P., Shetty, N., and Lim, T.-C., Automated diagnosis of glaucoma using digital fundus images. *J. Med. Syst.* 33(5):337, 2009.
19. Gayathri, R., and Rao, P. V., Glaucoma detection using cup to disc ratio and artificial neural networks. *International Journal of Engineering & Technology* 7:135–140, 2018.
20. Matsopoulos, G. K., Asvestas, P. A., Delibasis, K. K., Mouravliansky, N. A., and Zeyen, T. G., Detection of glaucomatous change based on vessel shape analysis. *Comput. Med. Imaging Graph.* 32(3):183–192, 2008.
21. Simonthomas, S., Thulasi, N., and Asharaf, P., Automated diagnosis of glaucoma using Haralick texture features. In Information Communication and Embedded Systems (ICICES), 2014 International Conference on, pp. 1–6. IEEE, 2014.
22. Fink, F., Worle, K., Gruber, P., Tome, A. M., Gorriz-Saez, J. M., Puntonet, C. G., and Lang, E. W., ICA analysis of retina images for glaucoma classification. In Engineering in Medicine and Biology Society, 2008. EMBS 2008. 30th Annual International Conference of the IEEE, pp. 4664–4667. IEEE, 2008.
23. Acharya, U. R., Bat, S., Koh, J. E. W., Bhandary, S. V., and Adeli, H., A novel algorithm to detect glaucoma risk using texton and local configuration pattern features extracted from fundus images. *Comput. Biol. Med.* 88:72–83, 2017.
24. Chen, Xiangyu, Xu, Yanwu, Wong, Damon Wing Kee, Wong, Tien Yin, and Liu, Jiang, Glaucoma Detection based on Deep Convolutional Neural Network, 37th Annual International IEEE conference on Engineering in Medicine and Biology Society (EMBC), 715–718, 2015.
25. Raghavendra, U., Bhandary, S. V., Gudigar, A., and Acharya, U. R., Novel expert system for glaucoma identification using non-parametric spatial envelope energy spectrum with fundus images. *Biocybernetics and Biomedical Engineering* 38(1):170–180, 2017.
26. Raghavendra, U., Fujita, H., Bhandary, S. V., Gudigar, A., Tan, J. H., and Acharya, U. R., Deep convolution neural network for accurate diagnosis of glaucoma using digital fundus images. *Inf. Sci.* 441:41–49, 2018.
27. Xu, Y., Xu, D., Lin, S., Liu, J., Cheng, J., Cheung, C., Aung, T., and Wong, T., Sliding window and regression based cup detection in digital fundus images for glaucoma diagnosis. *Medical Image Computing and Computer-Assisted Intervention–MICCAI* 2011: 1–8, 2011.
28. Dua, S., Acharya, U. R., Chowriappa, P., and Vinitha Sree, S., Wavelet-based energy features for glaucomatous image classification. *IEEE Trans. Inf. Technol. Biomed.* 16(1):80–87, 2012.
29. Acharya, U. R., Dua, S., Du, X., Sree, S. V., and Chua, C. K., Automated diagnosis of glaucoma using texture and higher order spectra features. *IEEE Trans Inf Technol Biomed* 15(3):449–455, 2011.
30. Chrástek, R., Wolf, M., Donath, K., Niemann, H., Paulus, D., Hothorn, T., Lausen, B., Lämmer, R., Mardin, C. Y., and Michelson, G., Automated segmentation of the optic nerve head for diagnosis of glaucoma. *Med. Image Anal.* 9(4):297–314, 2005.
31. Yin, Fengshou, Liu, Jiang, Wong, Damon Wing Kee, Tan, Ngan Meng, Cheung, Carol, Baskaran, Mani, Aung, Tin, and Wong, Tien Yin., Automated segmentation of optic disc and optic cup in fundus images for glaucoma diagnosis. In Computer-based medical systems (CBMS), 2012 25th international symposium on, pp. 1–6. IEEE, 2012.
32. Maheshwari, S., Pachori, R. B., Kanhangad, V., Bhandary, S. V., and Acharya, U. R., Iterative variational mode decomposition based automated detection of glaucoma using fundus images. *Comput. Biol. Med.* 88:142–149, 2017.
33. Maheshwari, S., Kanhangad, V., Pachori, R. B., Bhandary, S. V., and Acharya, U. R., Automated glaucoma diagnosis using bit-plane slicing and local binary pattern techniques. *Comput. Biol. Med.*, 2018 (In Press).
34. Olshausen, B. A., and Field, D. J., Sparse coding with an over complete basis set: A strategy employed by V1. Vis. Res. 37: 3311–3325, 1997.
35. Zhang, C., Cheng, X., Liu, J., He, J., and Liu, G., Deep sparse autoencoder for feature extraction and diagnosis of locomotive adhesion status. *Journal of Control Science and Engineering* 2018, Article ID 8676387:9. https://doi.org/10.1155/2018/8676387.
36. Yang, J., Bai, Y., Li, G., Liu, M., and Liu, X., A novel method of diagnosing premature ventricular contraction based on sparse autoencoder and softmax regression. *Biomed. Mater. Eng.* 26: S1549–S1558, 2015.
37. Chen, L., Zhou, M., Su, W., Wu, M., She, J., and Hirota, K., Softmax regression based deep sparse autoencoder network for facial emotion recognition in human-robot interaction. *Inf. Sci.* 428:49–61, 2018.
38. Shin, H.-C., Orton, M. R., Collins, D. J., Doran, S. J., and Leach, M. O., Stacked autoencoders for unsupervised feature learning and multiple organ detection in a pilot study using 4D patient data. *IEEE Trans. Pattern Anal. Mach. Intell.* 35(8):1930–1943, 2013.